

Density-Informed Pseudo-Counts for Calibrated Evidential Deep Learning

Pietro Carlotti^{*,†}, Nevena Gligić^{*,†} and Arya Farahi^{*}

Abstract. Evidential Deep Learning (EDL) is a popular framework for uncertainty-aware classification that models predictive uncertainty via Dirichlet distributions parameterized by neural networks. Despite its popularity, its theoretical foundations and behavior under distributional shift remain poorly understood. In this work, we provide a principled statistical interpretation by proving that EDL training corresponds to amortized variational inference in a hierarchical Bayesian model with a tempered pseudo-likelihood. This perspective reveals a major drawback: standard EDL conflates epistemic and aleatoric uncertainty, leading to systematic overconfidence on out-of-distribution (OOD) inputs. To address this, we introduce Density-Informed Pseudo-count EDL (DIP-EDL), a new parametrization that decouples class prediction from the magnitude of uncertainty by separately estimating the conditional label distribution and the marginal covariate density. This separation preserves evidence in high-density regions while shrinking predictions toward a uniform prior for OOD data. Theoretically, we prove that DIP-EDL achieves asymptotic concentration. Empirically, we show that our method enhances interpretability and improves robustness and uncertainty calibration under distributional shift.

1 Introduction

Uncertainty quantification is a central challenge in modern machine learning, particularly in safety-critical and high-stakes applications such as medical diagnosis [1] and scientific discovery [17]. While deep neural networks achieve remarkable predictive accuracy, they are notoriously prone to overconfidence [20], especially under limited data or distributional shift [44, 38]. Reliable uncertainty estimates are therefore essential for calibrated decision-making, detection of out-of-distribution (OOD) inputs, robust deployment, and supporting downstream reasoning. Despite its importance, principled, scalable uncertainty quantification for deep models remains an open problem.

A wide range of methods has been proposed to address this challenge [38, 24]. Bayesian neural networks aim to capture epistemic uncertainty by placing priors over model parameters and performing posterior inference, typically via variational approximations or Monte Carlo sampling [5, 25, 16]. Ensemble-based methods approximate posterior uncertainty by aggregating predictions from multiple trained models, yielding strong empirical performance at the cost of increased computational burden [31, 52]. Alternatively, post-hoc calibration methods adjust predictive confidence without explicitly modeling uncertainty [20, 19]. While effective in certain problems, these approaches

^{*}Department of Statistics and Data Sciences, The University of Texas at Austin, pietro.carlotti@utexas.edu; nevena.gligic@utexas.edu; arya.farahi@austin.utexas.edu

[†]Equal contribution.

often suffer from scalability, complex training pipelines, or limited interpretability of the resulting uncertainty estimates.

Evidential Deep Learning (EDL) has emerged as an alternative that directly models predictive uncertainty at the output level [46]. Rather than placing distributions over network parameters, EDL predicts a distribution over class probabilities parameterizing a Dirichlet distribution with a neural network. This formulation provides a unified representation of prediction confidence and uncertainty, allows for single forward-pass inference, and integrates naturally with standard deep learning pipelines. Hence, EDL has gained popularity as a practical framework for uncertainty-aware classification [18]. The main idea of EDL is to map the covariates $X \in \mathbb{R}^d$ to a distribution over the class probabilities $p \in \Delta^{K-1}$ for a categorical response variable $Y \in \{1, \dots, K\}$. The original formulation of Sensoy et al. [46] achieve this by specifying the distribution of the class probabilities using a Dirichlet distribution with concentration parameters given by a neural network $\text{NN}^\phi : \mathbb{R}^d \rightarrow \mathbb{R}_+^K$ with parameters ϕ which outputs a K -dimensional vector of non-negative weights.

To train this model, Sensoy et al. [46] propose a few different loss functions to minimize. All of these loss functions share the same structure:

$$\mathcal{L}_{\text{EDL}}^\lambda(\phi) = \mathcal{L}_{\text{data}}(\phi) + \lambda \mathcal{L}_{\text{reg}}(\phi), \quad (1)$$

where $\mathcal{L}_{\text{data}}(\cdot)$ is a data term that encourages the model to fit the training data, $\mathcal{L}_{\text{reg}}(\cdot)$ is a regularization term that penalizes complex models, and $\lambda > 0$ is a hyperparameter that controls the trade-off between data fit and regularization. In particular, we will focus on this specific choice of the data and regularization terms

$$\begin{aligned} \mathcal{L}_{\text{data}}(\phi) &= \sum_{i=1}^n -\mathbb{E}_{\text{Dir}(\alpha + \text{NN}_{X_i}^\phi)} [\log \text{Cat}(Y_i \mid p_i)], \\ \mathcal{L}_{\text{reg}}(\phi) &= \sum_{i=1}^n \text{KL} \left(\text{Dir} \left(\alpha + \text{NN}_{X_i}^\phi \right) \parallel \text{Dir}(\alpha) \right), \end{aligned} \quad (2)$$

where $\alpha \in \mathbb{R}_+^K$ is prior concentration parameters. Despite its intuitive appeal and empirical success, the theoretical foundations of EDL and its behavior under distributional shift remain poorly understood. In particular, it is unclear how the learned Dirichlet distributions relate to the underlying data-generating processes, and whether EDL can meaningfully distinguish among different sources of uncertainty. See Appendix A for a more detailed review.

In this work, we provide a statistical interpretation of the EDL framework, elucidate the role of the regularization parameter, and propose a novel parametrization, DIP-EDL, to improve performance under distributional shifts. DIP-EDL is a principled method that decouples class prediction from uncertainty magnitude by separately estimating conditional label distributions and marginal covariate densities.

2 Statistical Interpretation of EDL

Here, we present two alternative interpretations (i) a hierarchical Bayesian model with amortized variational inference, and (ii) an empirical risk minimization approach; and

show that both formulations lead to the same optimization objective used in EDL, providing a statistical interpretation and clarifying its uncertainty quantification properties.

2.1 Problem Setup and Notation

Suppose data is generated according to

$$(Y_i, X_i) \stackrel{\text{i.i.d.}}{\sim} P_{Y,X}^*, \quad i = 1, \dots, n. \quad (3)$$

The joint distribution admits the factorization $P_{Y,X}^* = P_{Y|X}^* P_X^*$, where $P_{Y|X}^*$ denotes the conditional distribution of Y given X , and P_X^* the marginal distribution of X . Throughout the analysis, we assume that P_X^* is absolutely continuous with respect to the Lebesgue measure on \mathbb{R}^d .

The aim of classification is to learn the conditional label distribution $P_{Y|X}^*$ from the observed data, both for in-sample points $i = 1, \dots, n$ and for unseen out-of-sample inputs $i \geq n + 1$, and to subsequently quantify the uncertainty associated with these learned conditional distributions.

2.2 Amortized Variational Inference

First, suppose a hierarchical Bayesian model in which class probabilities vary across observations.

Definition 2.1. Independent Categorical-Dirichlet Model. Let $\alpha \in \mathbb{R}_+^K$ be a vector of prior concentration parameters. The model is defined as follows $Y_i \mid p_i \stackrel{\text{ind.}}{\sim} f_{p_i} = \text{Cat}(p_i)$ and $p_i \stackrel{\text{i.i.d.}}{\sim} \pi = \text{Dir}(\alpha)$ for $i = 1, \dots, n$.

This choice of prior is convenient due to its conjugacy with the categorical likelihood; indeed, it is a well-known result that the posterior of the class probabilities can be computed in closed form, as summarized in the following proposition.

Proposition 2.2. *Suppose model in Definition 2.1, the posterior distribution of each vector of class probabilities is $p_i \mid Y_{1:n} \sim \pi_{Y_i} = \text{Dir}(\alpha + e_{Y_i})$ where e_{Y_i} denotes the one-hot encoding of Y_i . Furthermore, the joint posterior factorizes across observations $p_{1:n} \mid Y_{1:n} \sim \pi_{Y_{1:n}} = \prod_{i=1}^n \pi_{Y_i}$. Finally, the posterior predictive distribution is $Y_{n+1} \mid Y_{1:n} \sim \text{Cat}\left(\frac{\alpha}{\alpha_0}\right)$, where $\alpha_0 = \sum_{k=1}^K \alpha_k$.*

Despite the appealing computational tractability, two related challenges limit its practical applicability. (1) This specification neglects the covariates entirely, which is unrealistic in practice. (2) The class probabilities for each observation are informed solely by its observed label, and there is no borrowing of information. The second limitation is especially problematic for prediction within the support of the training distribution, as the posterior predictive reduces to the prior predictive. While returning to the prior is a desirable property for truly OOD data, this result implies that the model cannot generalize to new in-distribution observations. A natural way to address these limitations is to extend the hierarchical model to incorporate covariates.

Definition 2.3. Covariate-Indexed Categorical-Dirichlet Model. Let $\alpha \in \mathbb{R}_+^K$ be a vector of prior concentration parameters. The model is $Y_i | p_i \stackrel{\text{ind.}}{\sim} f_{p_i}, p_i = p_{X_i}, p_j \stackrel{\text{i.i.d.}}{\sim} \pi, X_i \stackrel{\text{i.i.d.}}{\sim} P_X^*$ for $j = 1, \dots, M_n$ and $i = 1, \dots, n$ where $M_n = |\{X_{1:n}\}|$ is the number of distinct covariate values.

As in the previous model, the Covariate-Indexed Categorical-Dirichlet Model retains conjugacy between the categorical likelihood and the Dirichlet prior, enabling closed-form posterior inference, as formalized in Proposition 2.4.

Proposition 2.4. *Given the model in Definition 2.3, the posterior distribution of each vector of class probabilities is $p_j | X_{1:n}, Y_{1:n} \sim \text{Dir}(\alpha + c_j)$, for $j = 1, \dots, M_n$, where $c_j = \sum_{i=1}^n \mathbb{I}(X_i = x_j^*) e_{Y_i}$ is the count vector of labels for observations with covariate value x_j^* , where $x_{1:M_n}^*$ are the distinct covariate values in $X_{1:n}$. Furthermore, the joint posterior factorizes across distinct covariate values $p_{1:M_n} | X_{1:n}, Y_{1:n} \sim \prod_{j=1}^{M_n} \text{Dir}(\alpha + c_j)$. Finally, the posterior predictive distribution for a new observation with covariate value $X_{n+1} = x$ is $Y_{n+1} | X_{1:n+1}, Y_{1:n} \sim \text{Cat}\left(\frac{\alpha + c_x}{\alpha_0 + S_x}\right)$, where $S_x = \sum_{k=1}^K c_x(k)$ and $c_x = \begin{cases} c_j & \text{if } x = x_j, \\ \mathbf{0}_K, & \text{otherwise.} \end{cases}$*

Although this model incorporates covariate information and is computationally tractable, it is limited to discrete covariates. In our setting, P_X^* is absolutely continuous, so each X_i is almost surely unique. Hence, there is no information sharing across observations, and inference reduces to that of the Independent Categorical-Dirichlet Model.

The model in Definition 2.3 does not overcome the limitations of the model in Definition 2.1. One option, albeit unconventional, is to retain the original model from Definition 2.1 and introduce covariate dependence via an approximate inference procedure. In particular, this can be achieved using amortized variational inference [37] to approximate the posterior of the class probabilities.

Definition 2.5. Amortized Variational Inference for the Independent Categorical-Dirichlet Model. Given the model in Definition 2.1. We approximate the posterior of the class probabilities $p_{1:n} | Y_{1:n} \approx \hat{q}_{X_{1:n}}$, where $\hat{q}_{X_{1:n}}$ minimizes the Kullback-Leibler (KL) divergence to the true posterior over a chosen variational family $\mathcal{Q}_{X_{1:n}}$. We have $\hat{q}_{X_{1:n}} = \arg \min_{q_{X_{1:n}} \in \mathcal{Q}_{X_{1:n}}} \{\text{KL}(q_{X_{1:n}} \| \pi_{Y_{1:n}})\}$, where $q_{X_{1:n}} \in \mathcal{Q}_{X_{1:n}}$ being a distribution over $(\Delta^{K-1})^n$ that may depend on the covariates $X_{1:n}$.

To mimic the factorization of the posterior across observations, we adopt a mean-field variational family $\mathcal{Q}_{X_{1:n}} = \{q_{X_{1:n}}^\phi : q_{X_{1:n}}^\phi = \prod_{i=1}^n q_{X_i}^\phi, \phi \in \Phi\}$, where each individual-level variational distribution is $q_{X_i}^\phi = \text{Dir}(\alpha + \text{NN}^\phi(X_i))$ and Φ denotes the parameter space defined by the architecture of a neural network $\text{NN}^\phi : \mathbb{R}^d \rightarrow \mathbb{R}_+^K$.

This formulation improves the Independent Categorical-Dirichlet Model by leveraging covariate information, learning from the training data, and generalizing to new observations, while retaining the computational tractability of the original Bayesian model. Under the variational approximation, we estimate the posterior predictive distribution.

Proposition 2.6. *Suppose model in Definition 2.1 and the variational approximation in Definition 2.5. Then the approximate predictive distribution is $Y_{n+1} | Y_{1:n}, X_{1:n+1} \approx \text{Cat} \left(\frac{\alpha + \text{NN}_{X_{n+1}}^{\hat{\phi}_n}}{\alpha_0 + S_{X_{n+1}}^{\hat{\phi}_n}} \right)$, where $S_{X_{n+1}}^{\hat{\phi}_n} = \sum_{k=1}^K \text{NN}_{X_{n+1}}^{\hat{\phi}_n}(k)$, and $\hat{\phi}_n$ are the learned neural network parameters:*

$$\hat{\phi}_n = \arg \min_{\phi \in \Phi} \left\{ \text{KL} \left(q_{X_{1:n}}^{\phi} \| \pi_{Y_{1:n}} \right) \right\}. \quad (4)$$

Now, we expand the KL divergence from Equation (4).

Proposition 2.7. *Suppose model in Definition 2.1 and the variational approximation in Definition 2.5, the optimization problem in Equation (4) is equivalent to minimizing the following objective function*

$$\sum_{i=1}^n -\mathbb{E}_{q_{X_i}^{\phi}} [\log f_{p_i}(Y_i)] + \text{KL} \left(q_{X_i}^{\phi} \| \pi \right). \quad (5)$$

We observe that this objective closely matches the EDL loss in Equation (1) introduced by Sensoy et al. [46], differing only by the absence of a hyperparameter λ on the KL term. This discrepancy can be resolved via a modification of the base model in Definition 2.1.

Definition 2.8. Tempered Independent Categorical-Dirichlet Model. Let $\alpha \in \mathbb{R}_+^K$ be a vector of prior concentration parameters and let $\nu > 0$ be a temperature parameter. The model is $p_i \stackrel{\text{ind.}}{\propto} f_{p_i}^{\nu}$, $p_i \stackrel{\text{i.i.d.}}{\sim} \pi$ for $i = 1, \dots, n$.

This modified model is motivated by using a tempered likelihood [4], which provides explicit control over the data's influence on the posterior via the parameter ν , thereby introducing an additional degree of freedom in the trade-off between data fit and regularization.

We note that for $\nu \neq 1$, the categorical likelihood, $f_{p_i}^{\nu}(Y_i) = \prod_{k=1}^{K-1} p_i^{\nu} \mathbb{I}(Y_i=k) = f_{p_i}^{\nu}(Y_i)$, is no longer normalized. This implies that to have a valid likelihood, we would need to renormalize $f_{p_i}^{\nu}$ with the following normalizing constant $\sum_{k=1}^K p_i^{\nu}(k)$, which depends on both the class probabilities p_i and the temperature parameter ν . Rather than renormalizing, we adopt a generalized Bayesian approach and treat the unnormalized likelihood as a pseudo-likelihood for posterior updating that is a standard strategy in generalized Bayesian inference and pseudo-posterior methods [51].

Proposition 2.9. *Given the model in Definition 2.8, the posterior distribution of each vector of class probabilities is $p_i | Y_{1:n} \sim \pi_{Y_i}^{\nu} = \text{Dir}(\alpha + \nu e_{Y_i})$ for $i = 1, \dots, n$. The joint posterior factorizes across observations $p_{1:n} | Y_{1:n} \sim \pi_{Y_{1:n}}^{\nu} = \prod_{i=1}^n \pi_{Y_i}^{\nu}$. The posterior predictive distribution is $Y_{n+1} | Y_{1:n} \sim \text{Cat} \left(\frac{\alpha}{\alpha_0} \right)$.*

As before, covariate dependence and predictive generalization can be achieved via the amortized variational inference from Definition 2.5, now applied to the tempered posterior from the model in Definition 2.8. Then, we reach a key result: this procedure is equivalent to training an EDL model with the loss function of Sensoy et al. [46].

Theorem 2.10. *Given the tempered model in Definition 2.8 and the amortized variational approximation of Definition 2.5, the optimization problem is equivalent to training an EDL model with regularization parameter $\lambda = \frac{1}{\nu}$:*

$$\hat{\phi}_n = \arg \min_{\phi \in \Phi} \left\{ \mathcal{L}_{\text{EDL}}^{\frac{1}{\nu}}(\phi; Y_{1:n}, X_{1:n}) \right\}. \quad (6)$$

This statistical interpretation clarifies both the objective optimized by EDL models and the nature of their uncertainty quantification. Since the network parameters are implicitly learned by minimizing a KL divergence, this framework yields a precise characterization of the conditions that the learned parameters satisfy at convergence.

Proposition 2.11. *Consider the tempered model from Definition 2.8 and the amortized variational approximation in Definition 2.5. Assume the neural network is sufficiently expressive and the optimization attains the global minimum of the objective. Then the learned parameters $\hat{\phi}_n$ satisfy*

$$\text{NN}_{X_i}^{\hat{\phi}_n} = \nu e_{Y_i}, \quad i = 1, \dots, n. \quad (7)$$

This result has a direct implication for uncertainty quantification. In particular, consider the following uncertainty measure introduced by Sensoy et al. [46].

Definition 2.12. Vacuity. Let p be a probability vector distributed according to a Dirichlet distribution with concentration parameters $\beta_X \in \mathbb{R}_+^K$, possibly depending on covariates $X \in \mathbb{R}^d$. The vacuity is defined as

$$u(\beta_X) = K/a_0 \quad \text{where} \quad a_0 = \sum_{k=1}^K \beta_X(k). \quad (8)$$

In this setting, perfect interpolation implies that the uncertainty associated with in-sample probability vectors is constant across all training points and is fully determined by the temperature parameter ν .

Proposition 2.13. *Given the tempered model in Definition 2.8 and the amortized variational approximation in Definition 2.5, if the neural network satisfies the perfect-interpolation condition in Equation (7), then*

$$u\left(\alpha + \text{NN}_{X_i}^{\hat{\phi}_n}\right) = \frac{K}{\alpha_0 + \nu}, \quad i = 1, \dots, n. \quad (9)$$

This shows that the EDL framework is fundamentally governed by the temperature parameter, and that its uncertainty quantification is spurious unless ν is chosen meaningfully. These results corroborate recent theoretical critiques of EDL. Specifically, Bengs et al. [2] and Shen et al. [47] demonstrate that the reliance on a hyper-parameter to balance likelihood evidence against prior regularization introduces a fundamental arbitrariness into the uncertainty quantification process which can be theoretically problematic. For example, aleatoric uncertainty should represent a fixed constant of irreducible noise inherent to the data, yet in EDL, it changes depending on a user-defined hyperparameter.

2.3 Empirical Risk Minimization

An alternative interpretation of the EDL framework arises from the perspective of empirical risk minimization. Specifically, consider the following statistical learning problem.

Definition 2.14. Evidential Deep Learning as Empirical Risk Minimization.

Let the data be generated as in Equation (3) and consider the following loss function $l^\nu(\phi; y, x) := \text{KL}(q_x^\phi \parallel \pi_y^\nu)$, where q_x^ϕ is defined as in Section 2.2 and π_y^ν is the tempered posterior from Definition 2.8. The goal is to learn the parameters ϕ by minimizing the empirical risk $\widehat{\mathcal{R}}_n^\nu(\phi) = \frac{1}{n} \sum_{i=1}^n l^\nu(\phi; Y_i, X_i)$. This is the in-sample expected risk $\mathcal{R}^\nu(\phi) = \mathbb{E}_{P_{Y|X}^*} [l^\nu(\phi; Y, X)]$.

This formulation clarifies that the EDL objective can be interpreted as an empirical estimator of an expected value.

Theorem 2.15. *Under the setup of Definition 2.14, the empirical risk is equivalent to the EDL loss function $\widehat{\mathcal{R}}_n^\nu(\phi) = \frac{\nu}{n} \mathcal{L}_{\text{EDL}}^{\frac{1}{\nu}}(\phi; Y_{1:n}, X_{1:n})$.*

This perspective helps us understand what quantities are targeted by the training objective of EDL models.

Theorem 2.16. *Under the setup of Definition 2.14, let ϕ^* be the minimizer of the expected risk: $\phi^* = \arg \min_{\phi \in \Phi} \{\mathcal{R}^\nu(\phi)\}$. Then, if the class of neural networks is sufficiently expressive, the optimal variational distribution satisfies $q_X^{\phi^*} = \text{Dir}(\alpha + \nu P_{Y|X}^*)$.*

This result demonstrates that, even with access to the true oracle model $P_{Y|X}^*$, both the optimal variational distribution and the vacuity-based uncertainty over class probabilities remain determined by the temperature parameter ν .

Proposition 2.17. *Suppose Definition 2.14, if the condition in Theorem 2.16 is met, then $u(\alpha + \nu P_{Y|X}^*) = \frac{K}{\alpha_0 + \nu}$.*

Thus, the temperature parameter governs the model's uncertainty independently of the data fit, and vacuity persists even as the sample size grows. As noted by Shen et al. [47], this highlights a limitation of EDL: it cannot distinguish epistemic from aleatoric uncertainty, since vacuity remains constant regardless of data quantity.

3 Choice of the Temperature Parameter

Given the role of the temperature parameter ν , careful selection is essential for reliable uncertainty quantification. Indeed, Theorem 2.16 shows that EDL does not jointly learn the conditional label distribution and its associated uncertainty. Rather, it learns the conditional distribution alone, while uncertainty quantification is entirely governed by ν . In this sense, EDL attempts to address multiple objectives simultaneously, but resolves only the predictive one.

We therefore avoid manually specifying ν or treating it as a hyperparameter tuned via cross-validation on some predictive metrics, which may be arbitrary. Instead, we seek

a statistically principled choice of ν . To this end, we ask: what properties should reliable uncertainty quantification satisfy? We propose the following two desiderata: **(i) Distributional awareness:** Uncertainty is higher in low-density regions of the covariate space and, *a fortiori*, outside the training distribution, reflecting limited information about the conditional label distribution in such regions. **(ii) Asymptotic consistency:** Epistemic uncertainty vanishes asymptotically, while aleatoric uncertainty may persist.

The intuition for these criteria arises from the optimal variational distribution in Theorem 2.16, which resembles the posterior of the Covariate-Indexed Categorical-Dirichlet Model (Definition 2.3). Interpreting $\nu P_{Y|X}^*$ as the label count vector for covariate X , ν acts as a pseudo-count for that covariate. However, this interpretation remains problematic, as ν is treated as a global parameter and thus does not depend on sample size or the covariate distribution.

To address this issue, we reconsider the Covariate-Indexed Categorical-Dirichlet Model. Since this model is unsuitable for continuous covariates, we aim to induce a notion of proximity among covariates so that similar observations can share information. For prediction, labels from nearby training points should reduce uncertainty, while regions with no nearby data should reflect increased uncertainty due to limited information. Building on this idea, given a sample of size n and considering a small neighborhood around a covariate X_i , the expected number of observations is approximately $n P_X^*(X_i)$, and the expected number of labels equal to class k is $n P_X^*(X_i) P_{Y|X}^*(k | X_i)$. This observation motivates a strategy for choosing ν .

Definition 3.1. Density-Informed Pseudo-count EDL (DIP-EDL). We propose a mean-field approach to conduct approximate inference on the vectors of class probabilities, with each individual-level distribution defined as

$$q_{X_i}^{\psi, \phi} = \text{Dir} \left(\alpha + n \text{DE}_{X_i}^{\psi} \text{NN}_{X_i}^{\phi} \right), \quad i = 1, \dots, n, \quad (10)$$

where $\text{DE}^{\psi} : \mathbb{R}^d \rightarrow \mathbb{R}_+$ is a density estimator for P_X^* with parameters ψ , and $\text{NN}^{\phi} : \mathbb{R}^d \rightarrow \mathbb{R}_+^K$ is a neural network estimator for $P_{Y|X}^*$ with parameters ϕ .

From an applied perspective, this specification is convenient for two reasons. First, it enables independent training of the density function and the neural network, making practical implementation straightforward. Second, it is architecture-agnostic: any density estimator and neural network models can be used, and they may be trained with any loss functions suitable for density estimation and classification, provided they approximately correctly learn the target distributions.

Moreover, this formulation satisfies both previously stated desiderata. (i, Distributional Awareness) in low-density regions with few nearby training samples the posterior predictive distribution contracts toward the prior. (ii, Asymptotic Consistency) q_{X_i} concentrates around the true conditional distribution $P_{Y|X}^*(\cdot | X_i)$ as $n \rightarrow \infty$ (see Theorem 3.2).

Theorem 3.2. *Let the data be generated as in Equation (3) and consider the variational distribution from Definition 3.1. Assume that the density estimator and neural network*

estimators are consistent, $\text{DE}_{X_i}^\psi \xrightarrow{P} P_X^*(X_i)$, $\text{NN}_{X_i}^\phi \xrightarrow{P} P_{Y|X}^*(\cdot | X_i)$, then, the approximate posterior distribution converges in probability to the true conditional distribution. For $p_i | X_{1:n}, Y_{1:n} \approx q_{X_i}^{\psi, \phi}$, we have that $p_i | X_{1:n}, Y_{1:n} \xrightarrow{P} P_{Y|X}^*(\cdot | X_i)$.

Using density functions for OOD uncertainty quantification has been explored by prior work, where the density of inputs or latent representations is used to improve epistemic or predictive uncertainty estimates [e.g., 39, 6, 53, 50]. What distinguishes this work from prior efforts is that we do not include a density function as an ad-hoc component to enforce epistemic uncertainty. Instead, the use of density in our method naturally emerges from the model formulation without externally imposing it on the model’s uncertainty mechanism, leading to a more principled uncertainty representation and better empirical performance.

DIP-EDL bears a close conceptual resemblance to Posterior Network [PostNet, 7] in that both methods specify the approximate posterior over class probabilities via density-based pseudo-counts rather than ad-hoc heuristics. However, the methods differ in their uncertainty decomposition. In PostNet, pseudo-counts are derived as estimates of $n P_Y^*(k) P_{Z(X)|Y=k}^*(X | k)$ for $k = 1, \dots, K$, where $Z(X)$ is the learned latent representation of input X , $P_{Z(X)|Y=k}^*$ is the class-conditional latent density for class k , and $P_Y^*(k)$ is the prior distribution over classes. In practice, PostNet models $P_{Z(X)|Y=k}^*$ using normalizing flows and estimates $n P_Y^*$ as the class counts in the training set. Consequently, PostNet yields evidence based on the latent likelihood of an input under each class, bypassing the need for explicit out-of-distribution examples. By contrast, in DIP-EDL, we express pseudo-counts as estimates of $n P_X^*(X) P_{Y|X}^*(k | X)$. DIP-EDL decomposes uncertainty via label-conditional and marginal data distributions in the input space. If the mapping $Z(X)$ is a bijection, both formulations are equivalent up to a change of variables. However, our approach offers three primary advantages:

- **Direct Calibration:** It ties uncertainty directly to observable predictive outputs, resulting in improved empirical performance (see Section 4.2).
- **Modularity:** Unlike PostNet, which requires joint training with a regularized Uncertain Cross-Entropy loss, DIP-EDL estimates the distributions separately, allowing for more flexible, modular training.
- **Efficiency:** DIP-EDL has the potential to be much more computationally efficient as it requires only a single density estimator for the entire input space rather than one per class, which might be a significant benefit when the number of classes is large.

4 Experiments

We evaluate the performance of DIP-EDL against established baselines for uncertainty quantification under distributional shift, with a focus on OOD detection.

4.1 Experimental Configuration

Datasets. Following standard practice in the OOD uncertainty quantification literature, we utilize **MNIST** [13] and **CIFAR-10** [29] as ID datasets. For OOD evaluation,

we employ datasets that represent varying degrees of distribution shift: **K-MNIST** [10] and **Omniglot** [30] for MNIST, and **CIFAR-100** [28] and **SVHN** [40] for CIFAR-10. This selection allows us to evaluate model performance on both near-OOD (e.g., digits vs. characters) and far-OOD tasks (e.g., digits vs natural images), following the literature.

Baselines. We benchmark performance against established Dirichlet-based uncertainty quantification methods: the standard **EDL** [8] and its variants, **R-EDL** [8] and **DAEDL** [53], as well as **PostNet** [7]. Our selection is primarily guided by the constraint that uncertainty estimation must be performed without access to OOD data during training, a requirement satisfied by our and the four selected baseline models. This ensures a fair comparison among approaches. Additionally, we focus on efficient, one-pass models that operate within a single forward pass. Consequently, we exclude computationally expensive approaches such as Deep Ensembles [31] or MC-Dropout [16]. Furthermore, comparative analysis in prior work [46, 7, 8, 53] have demonstrated that the selected baselines consistently outperform ensemble-based methods and other evidential frameworks, [e.g., \mathcal{I} -EDL, 11].

Implementation Details. To accommodate the varying complexity of the benchmark tasks, we tailor the model architectures for each dataset. For MNIST, we utilize a standard **LeNet-5** [32], following [46]. Density estimation is performed using a **Masked Autoregressive Flow (MAF)** [41] operating on the flattened pixel space. For CIFAR-10, we employ a modified **ResNet-18** [23] adapted for low-resolution inputs. For density estimation, we use **Gaussian Discriminant Analysis (GDA)** [21] fitted on the spectrally normalized 512-dimensional feature embeddings of the pre-trained ResNet-18, following DAEDL’s implementation. See Appendix C for details.

Performance Metrics. Following common practices in the OOD detection literature [8, 53, 7], we report three metrics. First, we evaluate performance using the standard **classification accuracy** on the ID test set. For OOD detection, we report **AUROC** and **AUPR**, which assess the model’s ability to rank OOD samples higher in uncertainty than ID samples, regardless of the absolute uncertainty values. For these calculations, OOD samples are treated as the positive class (label 1) and ID samples as the negative class (label 0). Unlike ranking-based metrics, the **Brier Score (BS)** assesses the magnitude of the predicted probabilities. On ID data, BS is computed against the ground truth one-hot label targets, while for OOD data, we compute BS against a uniform target distribution ($1/K$). This metric penalizes high-confidence predictions on unseen domains, even if they correctly rank those domains as uncertain.

4.2 Experiments with MNIST as ID dataset

Table 1 summarizes performance on the MNIST ID task, together with robustness under semantic (K-MNIST) and domain (Omniglot) shifts. Among the evaluated methods, **DIP-EDL** achieves the strongest ID performance, attaining the highest classification accuracy (99.53%) and the lowest ID Brier Score (0.01). This shows an improvement in

calibration compared to EDL (0.19) and DAEDL (0.02), and maintaining competitive predictive accuracy.

These calibration improvements translate to strong OOD detection performance. On both, DIP-EDL achieves a high AUROC of 0.99, outperforming DAEDL and improving upon standard EDL (0.91). On Omniglot, AUROC values are near-saturated for multiple methods, however, clear differences emerge when considering OOD calibration. In particular, DIP-EDL yields among the lowest OOD BS, while methods such as PostNet exhibit high OOD BS despite strong ranking performance. This indicates that DIP-EDL produces more reliable uncertainty estimates under distributional shift, assigning low confidence to samples drawn from regions of low data density.

Table 1: ID and OOD performance when models trained on MNIST. We evaluate ID accuracy and calibration, alongside OOD detection against K-MNIST (near-OOD) and Omniglot (far-OOD). Results are reported as $\mu \pm \sigma$ over 4 runs. DIP-EDL achieves the strongest ID performance and superior or competitive OOD performance across both OOD datasets.

Model	ID Performance		OOD Performance Metrics					
	Acc. (\uparrow)	BS (\downarrow)	AUROC (\uparrow)		AUPR (\uparrow)		OOD BS (\downarrow)	
			K-MNIST	Omniglot	K-MNIST	Omniglot	K-MNIST	Omniglot
EDL	0.9166 \pm 0.0498	0.1886 \pm 0.0434	0.9116 \pm 0.0340	0.9204 \pm 0.0477	0.8622 \pm 0.0588	0.8566 \pm 0.0778	0.0569 \pm 0.0080	0.0185 \pm 0.0032
R-EDL	0.9940 \pm 0.0005	0.0113 \pm 0.0009	0.9729 \pm 0.0014	0.9879 \pm 0.0026	0.9599 \pm 0.0025	0.9818 \pm 0.0055	0.1755 \pm 0.0192	0.0726 \pm 0.0372
DAEDL	0.9937 \pm 0.0005	0.0225 \pm 0.0014	0.9987 \pm 0.0003	0.9997 \pm 0.0002	0.9981 \pm 0.0006	0.9995 \pm 0.0002	0.0097 \pm 0.0018	0.0000 \pm 0.0000
PostNet	0.9925 \pm 0.0009	0.0117 \pm 0.0017	0.9602 \pm 0.0128	0.9936 \pm 0.0026	0.9570 \pm 0.0111	0.9862 \pm 0.0053	0.4922 \pm 0.0184	0.2816 \pm 0.0514
DIP-EDL	0.9953 \pm 0.0003	0.0081 \pm 0.0005	0.9997 \pm 0.0000	0.9998 \pm 0.0000	0.9995 \pm 0.0001	0.9996 \pm 0.0001	0.0013 \pm 0.0002	0.0000 \pm 0.0000

4.3 Experiments with CIFAR-10 as ID dataset

Table 2 reports ID performance on CIFAR-10 and OOD detection results on CIFAR-100 (near semantic shift) and SVHN (far domain shift). Compared to MNIST, CIFAR-10 is more challenging due to higher visual complexity and greater intra-class variability. Among the evaluated methods, DIP-EDL achieves the strongest ID performance, obtaining the highest classification accuracy (91.8%) and the lowest ID BS (0.13), indicating improved calibration while maintaining high predictive accuracy even as it scales to more complex image data.

For OOD detection, performance trends differ between near- and far-shift scenarios. On the far-OOD task (SVHN), DIP-EDL achieves the highest AUROC (0.91) and AUPR (0.96), thus, outperforming EDL (0.88 AUROC, 0.92 AUPR) and other baseline methods. On the near-OOD task (CIFAR-100), which shares a significant visual overlap with CIFAR-10, and as such, represents a more challenging setting, AUROC and AUPR scores are more closely matched across methods, with DAEDL achieving the highest AUROC (0.83 vs. 0.81) and DIP-EDL attaining the highest AUPR (0.79). These results demonstrate successful and reliable distributional shift detection by DIP-EDL.

Despite strong OOD detection performance, DIP-EDL exhibits higher OOD BS on CIFAR-10 compared to MNIST. This behavior stems from how OOD BS is defined in the absence of ground-truth labels, as the mean squared error between predicted class probabilities and a uniform target distribution. Defined in this way, OOD BS measures how close the predictions for OOD data are to saying “I don’t know”. Higher OOD

BS scores are, therefore, not an indication of degraded OOD detection capability but rather of higher confidence than the ideal case of uniform target distribution. In other words, while likelihood estimates remain informative, as evidenced by strong AUROC and AUPR, they are not sufficiently close to zero to fully counteract the classifier’s confidence, as is the case for MNIST experiments. (See Appendix D for a visualization of this.) We attribute this effect primarily to the increased difficulty of density estimation in high-dimensional and low-density regions (e.g., visually complex datasets such as CIFAR-10, CIFAR-100, and SVHN). This interpretation is supported by the ablation study (Section 4.4), where removing the training set size component of the model improves OOD BS without affecting AUROC or AUPR. Overall, these results suggest that OOD BS behavior reflects limitations of high-dimensional density estimation rather than a failure of DIP-EDL to detect distributional shift.

Table 2: **ID and OOD performance when models are trained on CIFAR-10.** We evaluate ID accuracy and calibration, alongside OOD detection against CIFAR-100 (near-OOD) and SVHN (far-OOD). Results are reported as $\mu \pm \sigma$ over 4 runs. DIP-EDL achieves the strongest ID performance and demonstrates robust detection capabilities. High OOD Brier Score for DIP-EDL comes from the fact that the density estimator is not able to capture all the details of complex, high-dimensional datasets. Thus, the likelihood estimates are not able to scale down the overconfidence of the discriminative classifier scaled up by n . See Section 4.3, 4.4, D for more details.

Model	ID Performance		OOD Performance Metrics					
	Acc. (\uparrow)	BS (\downarrow)	AUROC (\uparrow)		AUPR (\uparrow)		OOD BS (\downarrow)	
			CIFAR-100	SVHN	CIFAR-100	SVHN	CIFAR-100	SVHN
EDL	0.8137 \pm 0.0098	0.3310 \pm 0.0062	0.8180 \pm 0.0067	0.8771 \pm 0.0134	0.7577 \pm 0.0087	0.9195 \pm 0.0075	0.0654 \pm 0.0036	0.0235 \pm 0.0093
R-EDL	0.8963 \pm 0.0036	0.1718 \pm 0.0055	0.7359 \pm 0.0045	0.7584 \pm 0.0035	0.6923 \pm 0.0038	0.8561 \pm 0.0116	0.1166 \pm 0.0058	0.0735 \pm 0.0186
DAEDL	0.8892 \pm 0.0008	0.1742 \pm 0.0008	0.8337 \pm 0.0022	0.8596 \pm 0.0126	0.7919 \pm 0.0040	0.9077 \pm 0.0143	0.4125 \pm 0.0063	0.3924 \pm 0.0397
PostNet	0.8204 \pm 0.0054	0.2570 \pm 0.0059	0.7808 \pm 0.0055	0.8227 \pm 0.0332	0.7405 \pm 0.0091	0.8839 \pm 0.0232	0.4527 \pm 0.0085	0.4220 \pm 0.0339
DIP-EDL	0.9179 \pm 0.0022	0.1329 \pm 0.0029	0.8130 \pm 0.0039	0.9149 \pm 0.0207	0.7949 \pm 0.0056	0.9581 \pm 0.0135	0.6329 \pm 0.0038	0.5485 \pm 0.0474

4.4 Ablation Study

We conduct an ablation study to isolate the contributions of the three core components of the proposed DIP-EDL framework: (i) training set size, n , (ii) the density estimator, $DE_{X_i}^\psi$, and (iii) the discriminative classifier, $NN_{X_i}^\phi$. Table 3 reports results on MNIST and CIFAR-10 for pairwise combinations and the full model. For the full results, including isolating each individual component, see Appendix E.

The results show the distinct role of each component. In particular, the discriminative classifier, $NN_{X_i}^\phi$, affect ID predictive performance. Configurations that exclude $NN_{X_i}^\phi$ show near-random classification accuracy. The density estimator $DE_{X_i}^\psi$, is responsible for detecting distributional shift independently of class labels. Configurations that exclude this component achieve near-random OOD detection.

Finally, the training set size, n , acts as a scaling factor and is required for concentration (see Theorem 3.2). As such, is affect calibration but has no influence on ID accuracy or OOD detection. In particular, incorporating n scales up the predicted Dirichlet concentration parameters proportionally to the size of the training set, increasing model

Table 3: **Ablation study of DIP-EDL.** We evaluate the individual and combined contributions of training set size, n , the density estimator, $\text{DE}_{X_i}^\psi$, and the discriminative classifier, $\text{NN}_{X_i}^\phi$. The results demonstrate how the model splits its tasks across the three components and achieves the best performance when all three components are included.

Components	ID Performance				OOD Performance Metrics						
	Acc. (\uparrow)		BS (\downarrow)		AUROC (\uparrow)		AUPR (\uparrow)		OOD BS (\downarrow)		
	n	$\text{DE}_{X_i}^\psi$	$\text{NN}_{X_i}^\phi$	MNIST	K-MNIST	Omniglot	K-MNIST	Omniglot	K-MNIST	Omniglot	
✓	✓	✗		0.0980	0.9000	0.9998	0.9998	0.9996	0.9997	0.0000	0.0000
✓	✗	✓		0.9958	0.0069	0.5138	0.5299	0.5742	0.6408	0.6826	0.7124
✗	✓	✓		0.9952	0.7202	0.9996	0.9996	0.9992	0.9994	0.0000	0.0000
✓	✓	✓		0.9955	0.0079	0.9998	0.9998	0.9995	0.9997	0.0014	0.0000
<hr/>											
<hr/>											

regularization parameter’s role and exposes a fundamental limitation in standard EDL: its inability to faithfully quantify uncertainty, resulting in overconfidence on ID and OOD data.

To address this, we introduced DIP-EDL, which decouples class prediction from uncertainty by scaling pseudo-counts with marginal covariate density. This model allows distributional awareness and asymptotic consistency. Theoretically, we proved that DIP-EDL satisfies asymptotic concentration, guaranteeing the posterior converges to the true conditional distribution. Empirically, we show DIP-EDL outperformed established baselines (EDL, R-EDL, DAEDL, PostNet) in ID calibration and OOD detection on MNIST and CIFAR-10.

Future research could explore more sophisticated density estimators and establish finite-sample convergence rates. Ultimately, DIP-EDL demonstrates that grounding deep learning in statistical theory yields both rigorous insights and superior predictive robustness.

Impact Statement

This work improves machine learning models’ ability to quantify epistemic predictive uncertainty in data-driven problems. This is a necessary feature for deploying reliable AI in real-world environments, where data shifts can lead to silent failures. However, interpreting uncertainty estimates may be challenging for end users, and misinterpretation could lead to inappropriate trust, misuse, or suboptimal decision-making if not accompanied by proper guidance and evaluation [43, 27, 33].

References

- [1] Begoli, E., Bhattacharya, T., and Kusnezov, D. (2019). “The need for uncertainty quantification in machine-assisted medical decision making.” *Nature Machine Intelligence*, 1(1): 20–23. [1](#)
- [2] Bengs, V., Hüllermeier, E., and Waegeman, W. (2022). “Pitfalls of epistemic uncertainty quantification through loss minimisation.” *Advances in Neural Information Processing Systems*, 35: 29205–29216. [6](#), [21](#)
- [3] — (2023). “On second-order scoring rules for epistemic uncertainty quantification.” In *International Conference on Machine Learning*, 2078–2091. PMLR. [21](#)
- [4] Bissiri, P. G., Holmes, C. C., and Walker, S. G. (2016). “A general framework for updating belief distributions.” *Journal of the Royal Statistical Society Series B: Statistical Methodology*, 78(5): 1103–1130. [5](#)
- [5] Blundell, C., Cornebise, J., Kavukcuoglu, K., and Wierstra, D. (2015). “Weight uncertainty in neural network.” In *International conference on machine learning*, 1613–1622. PMLR. [1](#)
- [6] Bui, H. M. and Liu, A. (2024). “Density-regression: Efficient and distance-aware deep regressor for uncertainty estimation under distribution shifts.” In *International Conference on Artificial Intelligence and Statistics*, 2998–3006. PMLR. [9](#)
- [7] Charpentier, B., Zügner, D., and Günnemann, S. (2020). “Posterior network: uncertainty estimation without OOD samples via density-based pseudo-counts.” In *Proceedings of the 34th International Conference on Neural Information Processing Systems*, NIPS ’20. Red Hook, NY, USA: Curran Associates Inc. [9](#), [10](#), [20](#), [32](#)
- [8] Chen, M., Gao, J., and Xu, C. (2024). “R-EDL: Relaxing Nonessential Settings of Evidential Deep Learning.” In *The Twelfth International Conference on Learning Representations*.
URL <https://openreview.net/forum?id=Si3YFA641c> [10](#), [32](#)
- [9] — (2024). “R-edl: Relaxing nonessential settings of evidential deep learning.” In *The Twelfth International Conference on Learning Representations*. [21](#)
- [10] Clanuwat, T., Bober-Irizar, M., Kitamoto, A., Lamb, A., Yamamoto, K., and Ha, D. (2018). “Deep Learning for Classical Japanese Literature.” [10](#)
- [11] Deng, D., Chen, G., Yu, Y., Liu, F., and Heng, P.-A. (2023). “Uncertainty Estimation by Fisher Information-based Evidential Deep Learning.”
URL <https://arxiv.org/abs/2303.02045> [10](#)
- [12] — (2023). “Uncertainty estimation by fisher information-based evidential deep learning.” In *International conference on machine learning*, 7596–7616. PMLR. [20](#)
- [13] Deng, L. (2012). “The MNIST Database of Handwritten Digit Images for Machine Learning Research [Best of the Web].” *IEEE Signal Processing Magazine*, 29(6): 141–142. [9](#), [29](#)
- [14] Durkan, C., Bekasov, A., Murray, I., and Papamakarios, G. (2020). “nflows: nor-

- malizing flows in PyTorch.” URL <https://doi.org/10.5281/zenodo.4296287> 29
- [15] Fathullah, Y. and Gales, M. J. (2022). “Self-distribution distillation: efficient uncertainty estimation.” In *Uncertainty in Artificial Intelligence*, 663–673. PMLR. 20
- [16] Gal, Y. and Ghahramani, Z. (2016). “Dropout as a bayesian approximation: Representing model uncertainty in deep learning.” In *international conference on machine learning*, 1050–1059. PMLR. 1, 10
- [17] Gal, Y., Koumoutsakos, P., Lanusse, F., Louppe, G., and Papadimitriou, C. (2022). “Bayesian uncertainty quantification for machine-learned models in physics.” *Nature Reviews Physics*, 4(9): 573–577. 1
- [18] Gao, J., Chen, M., Xiang, L., and Xu, C. (2025). “A comprehensive survey on evidential deep learning and its applications.” *IEEE Transactions on Pattern Analysis and Machine Intelligence*. 2
- [19] Gibbs, I., Cherian, J. J., and Candès, E. J. (2025). “Conformal prediction with conditional guarantees.” *Journal of the Royal Statistical Society Series B: Statistical Methodology*, qkaf008. 1
- [20] Guo, C., Pleiss, G., Sun, Y., and Weinberger, K. Q. (2017). “On calibration of modern neural networks.” In *International conference on machine learning*, 1321–1330. PMLR. 1, 13
- [21] Hastie, T. J. and Tibshirani, R. (1996). “Discriminant Analysis by Gaussian Mixtures.” *Journal of the royal statistical society series b-methodological*, 58: 155–176. URL <https://api.semanticscholar.org/CorpusID:118694839> 10
- [22] Haussmann, M., Gerwinn, S., and Kandemir, M. (2019). “Bayesian evidential deep learning with PAC regularization.” *arXiv preprint arXiv:1906.00816*. 20
- [23] He, K., Zhang, X., Ren, S., and Sun, J. (2016). “Deep Residual Learning for Image Recognition.” In *2016 IEEE Conference on Computer Vision and Pattern Recognition (CVPR)*, 770–778. 10, 31
- [24] He, W., Jiang, Z., Xiao, T., Xu, Z., and Li, Y. (2025). “A survey on uncertainty quantification methods for deep learning.” *ACM Computing Surveys*. 1
- [25] Hernández-Lobato, J. M. and Adams, R. (2015). “Probabilistic backpropagation for scalable learning of bayesian neural networks.” In *International conference on machine learning*, 1861–1869. PMLR. 1
- [26] Hinton, G., Vinyals, O., and Dean, J. (2015). “Distilling the knowledge in a neural network.” *arXiv preprint arXiv:1503.02531*. 20
- [27] Kerr, J., Van Der Bles, A.-M., Dryhurst, S., Schneider, C. R., Chopurian, V., Freeman, A. L., and Van Der Linden, S. (2023). “The effects of communicating uncertainty around statistics, on public trust.” *Royal Society Open Science*, 10(11): 230604. 14

- [28] Krizhevsky, A. (2009). “Learning Multiple Layers of Features from Tiny Images.” [10](https://www.semanticscholar.org/CorpusID:16852518)
- [29] Krizhevsky, A., Hinton, G., et al. (2009). “Learning multiple layers of features from tiny images.(2009).” [9, 31](https://www.semanticscholar.org/CorpusID:16852518)
- [30] Lake, B. M., Salakhutdinov, R., and Tenenbaum, J. B. (2015). “Human-level concept learning through probabilistic program induction.” *Science*, 350(6266): 1332–1338.
URL <https://www.semanticscholar.org/CorpusID:16852518> 10
- [31] Lakshminarayanan, B., Pritzel, A., and Blundell, C. (2017). “Simple and scalable predictive uncertainty estimation using deep ensembles.” *Advances in neural information processing systems*, 30. [1, 10](https://www.semanticscholar.org/CorpusID:16852518)
- [32] Lecun, Y., Bottou, L., Bengio, Y., and Haffner, P. (1998). “Gradient-based learning applied to document recognition.” *Proceedings of the IEEE*, 86(11): 2278–2324. [10, 29](https://www.semanticscholar.org/CorpusID:16852518)
- [33] Li, J., Yang, Y., Liao, Q. V., Zhang, J., and Lee, Y.-C. (2025). “As Confidence Aligns: Understanding the Effect of AI Confidence on Human Self-confidence in Human-AI Decision Making.” In *Proceedings of the 2025 CHI Conference on Human Factors in Computing Systems*, 1–16. [14](https://www.semanticscholar.org/CorpusID:16852518)
- [34] Malinin, A. and Gales, M. (2018). “Predictive uncertainty estimation via prior networks.” *Advances in neural information processing systems*, 31. [20](https://www.semanticscholar.org/CorpusID:16852518)
- [35] — (2019). “Reverse kl-divergence training of prior networks: Improved uncertainty and adversarial robustness.” *Advances in neural information processing systems*, 32. [20](https://www.semanticscholar.org/CorpusID:16852518)
- [36] Malinin, A., Mlodozeniec, B., and Gales, M. (2019). “Ensemble distribution distillation.” *arXiv preprint arXiv:1905.00076*. [20](https://www.semanticscholar.org/CorpusID:16852518)
- [37] Margossian, C. C. and Blei, D. M. (2023). “Amortized variational inference: When and why?” *arXiv preprint arXiv:2307.11018*. [4](https://www.semanticscholar.org/CorpusID:16852518)
- [38] Mucsányi, B., Kirchhof, M., and Oh, S. J. (2024). “Benchmarking uncertainty disentanglement: Specialized uncertainties for specialized tasks.” *Advances in neural information processing systems*, 37: 50972–51038. [1](https://www.semanticscholar.org/CorpusID:16852518)
- [39] Mukhoti, J., Kirsch, A., van Amersfoort, J., Torr, P. H., and Gal, Y. (2021). “Deep deterministic uncertainty: A simple baseline.” *arXiv preprint arXiv:2102.11582*. [9](https://www.semanticscholar.org/CorpusID:16852518)
- [40] Netzer, Y., Wang, T., Coates, A., Bissacco, A., Wu, B., and Ng, A. (2011). “Reading Digits in Natural Images with Unsupervised Feature Learning.”
URL <https://www.semanticscholar.org/CorpusID:16852518> 10
- [41] Papamakarios, G., Pavlakou, T., and Murray, I. (2017). “Masked Autoregressive Flow for Density Estimation.” In Guyon, I., Luxburg, U. V., Bengio, S., Wallach, H., Fergus, R., Vishwanathan, S., and Garnett, R. (eds.), *Advances in Neural Information Processing Systems*, volume 30. Curran Associates, Inc.

- URL https://proceedings.neurips.cc/paper_files/paper/2017/file/6c1da886822c67822bcf3679d04369fa-Paper.pdf 10, 29, 30
- [42] Paszke, A., Gross, S., Massa, F., Lerer, A., Bradbury, J., Chanan, G., Killeen, T., Lin, Z., Gimelshein, N., Antiga, L., Desmaison, A., Köpf, A., Yang, E., DeVito, Z., Raison, M., Tejani, A., Chilamkurthy, S., Steiner, B., Fang, L., Bai, J., and Chintala, S. (2019). *PyTorch: an imperative style, high-performance deep learning library*. Red Hook, NY, USA: Curran Associates Inc. 29
- [43] Schneider, C. R., Freeman, A. L., Spiegelhalter, D., and van der Linden, S. (2022). “The effects of communicating scientific uncertainty on trust and decision making in a public health context.” *Judgment and Decision Making*, 17(4): 849–882. 14
- [44] Seligmann, F., Becker, P., Volpp, M., and Neumann, G. (2023). “Beyond deep ensembles: A large-scale evaluation of bayesian deep learning under distribution shift.” *Advances in Neural Information Processing Systems*, 36: 29372–29405. 1
- [45] Sensoy, M., Kaplan, L., Cerutti, F., and Saleki, M. (2020). “Uncertainty-aware deep classifiers using generative models.” In *Proceedings of the AAAI conference on artificial intelligence*, volume 34, 5620–5627. 20
- [46] Sensoy, M., Kaplan, L., and Kandemir, M. (2018). “Evidential deep learning to quantify classification uncertainty.” *Advances in neural information processing systems*, 31. 2, 5, 6, 10, 20, 32
- [47] Shen, M., Ryu, J. J., Ghosh, S., Bu, Y., Sattigeri, P., Das, S., and Wornell, G. (2024). “Are uncertainty quantification capabilities of evidential deep learning a mirage?” *Advances in Neural Information Processing Systems*, 37: 107830–107864. 6, 7, 20, 21
- [48] Tsiligkaridis, T. (2021). “Information robust dirichlet networks for predictive uncertainty estimation.” US Patent App. 17/064,046. 20
- [49] Ulmer, D., Hardmeier, C., and Frellsen, J. (2021). “Prior and posterior networks: A survey on evidential deep learning methods for uncertainty estimation.” *arXiv preprint arXiv:2110.03051*. 20
- [50] Van Katwyk, P. and Bergen, K. J. (2025). “HybridFlow: Quantification of Aleatoric and Epistemic Uncertainty with a Single Hybrid Model.” *arXiv preprint arXiv:2510.05054*. 9
- [51] Ventura, L. and Racugno, W. (2016). “Pseudo-likelihoods for Bayesian inference.” In *Topics on methodological and applied statistical inference*, 205–220. Springer. 5
- [52] Wang, H. and Ji, Q. (2023). “Diversity-enhanced probabilistic ensemble for uncertainty estimation.” In *Uncertainty in Artificial Intelligence*, 2214–2225. PMLR. 1
- [53] Yoon, T. and Kim, H. (2024). “Uncertainty estimation by density aware evidential deep learning.” In *Proceedings of the 41st International Conference on Machine Learning*, ICML’24. JMLR.org. 9, 10, 31, 32

- [54] Zhao, X., Ou, Y., Kaplan, L., Chen, F., and Cho, J.-H. (2019). “Quantifying classification uncertainty using regularized evidential neural networks.” *arXiv preprint arXiv:1910.06864*. [20](#)

Appendix A: Related Literature.

This section contextualizes the proposed DIP-EDL method within the broader landscape of uncertainty quantification with EDL approaches. We first contrast our approach with existing EDL paradigms before summarizing the critical shortcomings identified in current EDL literature. For extensive surveys, we refer the reader to Ulmer et al. [49] for EDL-specific developments and Shen et al. [47] for a comprehensive overview of existing limitations.

A.1 Contrasting DIP-EDL with Existing EDL Paradigms

Following the taxonomy by Ulmer et al. [49], EDL methods for Dirichlet-based classification are primarily distinguished by two criteria: (i) whether the network parameterizes the prior or the posterior Dirichlet distribution, and (ii) whether the training process incorporates OOD samples to enforce uncertainty calibration.

Regarding the first criterion, Ulmer et al. [49] distinguish between *prior* and *posterior* networks. While both share a common optimization objective, balancing a predictive loss (e.g., cross-entropy) with an uncertainty-promoting regularizer (e.g., KL divergence toward a flat Dirichlet), their modeling mechanisms differ. Prior networks [22, 48] parameterize an input-dependent concentration vector that defines a Dirichlet prior and derive the posterior via Bayes’ theorem given the observed labels. Conversely, posterior networks [46, 7] bypass the explicit Bayesian update by directly predicting the pseudo-counts that define the concentration parameters of the Dirichlet posterior.

As for the second criterion, the idea is to train a model to output sharp Dirichlet distributions for in-distribution data and flat Dirichlet distributions for OOD data. Therefore, to achieve this kind of uncertainty calibration, the loss function is augmented with an additional regularization term, typically a KL divergence measure between the predicted Dirichlet distribution and a flat Dirichlet distribution, that penalizes confident predictions on OOD samples. In this paradigm, training is agnostic to the network type and can be applied to both prior [34, 35] and posterior [54, 45] network architectures.

While the aforementioned criteria categorize most EDL classification methods, certain approaches based on knowledge distillation [26] fall outside this taxonomy. These methods transfer uncertainty estimates from a complex teacher model to a more efficient student EDL model, training the latter to mimic the teacher’s distributional output. Notable examples include Malinin et al. [36], which distills the diversity of an ensemble into a single Dirichlet model, and Fathullah and Gales [15], which leverages self-distillation from Gaussian stochastic dropout.

Another notable departure from the standard taxonomy is the Fisher Information-based EDL framework proposed by Deng et al. [12]. This approach leverages the Fisher information of the Dirichlet distribution to quantify the informativeness of the evidence provided by each observation. By incorporating this metric, the model adjusts its concentration parameters, enhancing its sensitivity to evidence associated with uncertain or underrepresented classes.

A.2 Shortcomings of Existing EDL Approaches

Despite the growing popularity of EDL, several studies have identified fundamental limitations that challenge its ability to provide reliable uncertainty estimates. These critiques are summarized below.

More specifically, Bengs et al. [2] demonstrated that loss minimization is not a theoretically viable framework for learning distributions over probability distributions, such as the Dirichlet distributions employed in EDL. A critical consequence of this result is that the distributional uncertainty in EDL models fails to vanish even in the asymptotic limit of infinite training data. Bengs et al. [3] further extended this critique, proving that no loss function can successfully incentivize a second-order model to faithfully represent its epistemic uncertainty.

In a more recent theoretical analysis, Shen et al. [47] generalized previous critiques by characterizing the optimal distribution targeted by standard EDL models. They demonstrated that this distribution depends fundamentally on a sample-size-independent regularization coefficient, leading to two critical conclusions: (i) EDL models fail to faithfully represent aleatoric uncertainty, as its quantification is governed by an arbitrary hyperparameter rather than solely by the data-generating process; and (ii) they cannot reliably capture epistemic uncertainty, because the predicted Dirichlet distributions fail to concentrate around the true conditional distribution—even in the asymptotic limit—due to this persistent dependence on the regularization term.

Other works, such as Chen et al. [9] have also correctly identified the issue of the fundamental dependence of EDL models on a regularization hyperparameter and proposed possible remedies to it. In particular, Chen et al. [9] introduced R-EDL, treats the regularization hyperparameter as an adjustable hyperparameter, as opposed to a fixed constant, and tunes it with respect to some performance metric (e.g., OOD detection AUROC) over a validation set. While this approach improves empirical performance, it does not address the fundamental theoretical limitations of EDL models identified in prior works.

Appendix B: Proofs and Additional Derivations

We provide proofs for all propositions and theorems stated in the main text. We begin with the following lemma on the properties of the Dirichlet distribution, which is stated without proof, as it is a standard result.

Lemma B.1. *Expectation of the Dirichlet Distribution.* *Let $p \sim \text{Dir}(\beta)$ be a random vector distributed according to a Dirichlet distribution with concentration parameters $\beta \in \mathbb{R}_+^K$. Then, for each $k = 1, \dots, K$, we have that*

$$\mathbb{E}[p(k)] = \frac{\beta(k)}{\beta_0},$$

where $\beta_0 = \sum_{k=1}^K \beta(k)$.

B.1 Proof of Proposition 2.2

Proof. By Bayes' theorem, the posterior distribution of the class probabilities for each observation satisfies the following:

$$\begin{aligned}\pi_{Y_i}(p_i) &\propto f_{p_{1:n}}(Y_{1:n}) \pi(p_{1:n}) \\ &\propto f_{p_i}(Y_i) \pi(p_i) \\ &\propto \prod_{k=1}^K p_i(k)^{\mathbb{I}(Y_i=k)} \prod_{k=1}^K p_i(k)^{\alpha(k)-1} \\ &= \prod_{k=1}^K p_i(k)^{\alpha(k)+\mathbb{I}(Y_i=k)-1}.\end{aligned}$$

We recognize this as the kernel of a Dirichlet distribution with concentration parameters $\alpha + e_{Y_i}$, which implies that

$$p_i \mid Y_{1:n} \sim \pi_{Y_i} = \text{Dir}(\alpha + e_{Y_i}).$$

Furthermore, since the likelihood and prior factorize across observations, the joint posterior also factorizes:

$$\pi_{Y_{1:n}}(p_{1:n}) \propto f_{p_{1:n}}(Y_{1:n}) \pi(p_{1:n}) \propto \prod_{i=1}^n f_{p_i}(Y_i) \pi(p_i) \propto \prod_{i=1}^n \pi_{Y_i}(p_i).$$

As a consequence, the posterior distribution of new class probabilities is equal to the prior:

$$\pi_{Y_{1:n}}(p_{n+1}) \propto \prod_{i=1}^n f_{p_i}(Y_i) \prod_{i=1}^{n+1} \pi(p_i) \propto \pi(p_{n+1}) = \text{Dir}(\alpha).$$

Finally, the posterior predictive distribution follows from Lemma B.1:

$$\begin{aligned}\mathbb{P}(Y_{n+1} = k \mid Y_{1:n}) &= \int \mathbb{P}(Y_{n+1} = k \mid p_{n+1}) \pi_{Y_{1:n}}(p_{n+1}) dp_{n+1} \\ &= \int p_{n+1}(k) \pi(p_{n+1}) dp_{n+1} \\ &= \mathbb{E}_\pi[p_{n+1}(k)] \\ &= \frac{\alpha(k)}{\alpha_0}.\end{aligned}$$

□

B.2 Proof of Proposition 2.4

Proof. By Bayes' theorem, the posterior distribution of the class probabilities for each observation satisfies the following:

$$\pi_{X_{1:n}, Y_{1:n}}(p_j) \propto f_{p_{1:M_n}}(Y_{1:n} \mid X_{1:n}) \pi(p_{1:M_n} \mid X_{1:n})$$

$$\begin{aligned}
&= \prod_{i:X_i=x_j^*} f_{p_j}(Y_i) \pi(p_j) \\
&\propto \prod_{k=1}^K p_j(k)^{\sum_{i:X_i=x_j^*} \mathbb{I}(Y_i=k)} \prod_{k=1}^K p_j(k)^{\alpha(k)-1} \\
&= \prod_{k=1}^K p_j(k)^{\alpha(k)+c_j(k)-1}.
\end{aligned}$$

We recognize this as the kernel of a Dirichlet distribution with concentration parameters $\alpha + c_j$, which implies that

$$p_j \mid X_{1:n}, Y_{1:n} \sim \pi_{X_{1:n}, Y_{1:n}} = \text{Dir}(\alpha + c_j).$$

Furthermore, since the likelihood and prior factorize across unique covariate values, the joint posterior also factorizes:

$$\pi_{X_{1:n}, Y_{1:n}}(p_{1:M_n}) \propto f_{p_{1:M_n}}(Y_{1:n} \mid X_{1:n}) \pi(p_{1:M_n} \mid X_{1:n}) \propto \prod_{j=1}^{M_n} f_{p_j}(Y_{i:X_i=x_j^*}) \pi(p_j) \propto \prod_{j=1}^{M_n} \pi_{X_{1:n}, Y_{1:n}}(p_j).$$

As a consequence, the posterior distribution of new class probabilities is equal to the prior if the covariate is new and to the corresponding posterior if the covariate has been observed:

$$\begin{aligned}
\pi_{X_{1:n+1}, Y_{1:n}}(p_{n+1}) &\propto f_{p_{1:M_n}}(Y_{1:n} \mid X_{1:n}) \pi(p_{1:M_n}, p_{n+1} \mid X_{1:n+1}) \\
&\propto \begin{cases} \pi(p_{n+1}) = \text{Dir}(\alpha), & \text{if } X_{n+1} \notin \{X_{1:n}\}, \\ \pi_{X_{1:n}, Y_{1:n}}(p_j) = \text{Dir}(\alpha + c_j), & \text{if } X_{n+1} = x_j^* \text{ for some } j = 1, \dots, M_n. \end{cases}
\end{aligned}$$

Finally, the posterior predictive distribution follows from Lemma B.1:

$$\begin{aligned}
\mathbb{P}(Y_{n+1} = k \mid X_{1:n+1}, Y_{1:n}) &= \int \mathbb{P}(Y_{n+1} = k \mid p_{n+1}) \pi_{X_{1:n+1}, Y_{1:n}}(p_{n+1}) dp_{n+1} \\
&= \int p_{n+1}(k) \pi_{X_{1:n+1}, Y_{1:n}}(p_{n+1}) dp_{n+1} \\
&= \mathbb{E}_{\pi_{X_{1:n+1}, Y_{1:n}}}[p_{n+1}(k)] \\
&= \begin{cases} \frac{\alpha(k)}{\alpha_0}, & \text{if } X_{n+1} \notin \{X_{1:n}\}, \\ \frac{\alpha(k) + c_j(k)}{\alpha_0 + \sum_{k=1}^K c_j(k)}, & \text{if } X_{n+1} = x_j^* \text{ for some } j = 1, \dots, M_n. \end{cases}
\end{aligned}$$

□

B.3 Proof of Proposition 2.6

Proof. By Definition 2.5, the approximate posterior distribution of new class probabilities is as follows:

$$p_{n+1} \mid X_{n+1} \approx q_{X_{n+1}}^{\hat{\phi}_n} = \text{Dir} \left(\alpha + \text{NN}_{X_{n+1}}^{\hat{\phi}_n} \right).$$

Therefore, the posterior predictive distribution follows from Lemma B.1:

$$\begin{aligned}
\mathbb{P}(Y_{n+1} = k \mid X_{1:n+1}, Y_{1:n}) &= \int \mathbb{P}(Y_{n+1} = k \mid p_{n+1}) q_{X_{n+1}}^{\hat{\phi}}(p_{n+1}) dp_{n+1} \\
&= \int p_{n+1}(k) q_{X_{n+1}}^{\hat{\phi}}(p_{n+1}) dp_{n+1} \\
&= \mathbb{E}_{q_{X_{n+1}}^{\hat{\phi}}}[p_{n+1}(k)] \\
&= \frac{\alpha(k) + \text{NN}_{X_{n+1}}^{\hat{\phi}}(k)}{\alpha_0 + \sum_{k=1}^K \text{NN}_{X_{n+1}}^{\hat{\phi}}(k)}.
\end{aligned}$$

□

B.4 Proof of Proposition 2.7

Proof. Since both the variational distribution and the posterior factorize across observations, we have that

$$\begin{aligned}
\text{KL}\left(q_{X_{1:n}}^{\phi} \parallel \pi_{Y_{1:n}}\right) &= \mathbb{E}_{q_{X_{1:n}}^{\phi}} \left[\log \frac{\prod_{i=1}^n q_{X_i}^{\phi}(p_i)}{\prod_{i=1}^n \pi_{Y_i}(p_i)} \right] \\
&= \sum_{i=1}^n \mathbb{E}_{q_{X_i}^{\phi}} \left[\log \frac{q_{X_i}^{\phi}(p_i)}{\pi_{Y_i}(p_i)} \right] \\
&\propto \sum_{i=1}^n \mathbb{E}_{q_{X_i}^{\phi}} \left[\log \frac{q_{X_i}^{\phi}(p_i)}{f_{p_i}(Y_i) \pi(p_i)} \right] \\
&= \sum_{i=1}^n -\mathbb{E}_{q_{X_i}^{\phi}} [\log f_{p_i}(Y_i)] + \mathbb{E}_{q_{X_i}^{\phi}} \left[\log \frac{q_{X_i}^{\phi}(p_i)}{\pi(p_i)} \right] \\
&= \sum_{i=1}^n -\mathbb{E}_{q_{X_i}^{\phi}} [\log f_{p_i}(Y_i)] + \text{KL}\left(q_{X_i}^{\phi} \parallel \pi\right).
\end{aligned}$$

□

B.5 Proof of Proposition 2.9

Proof. The proof follows the same steps as in the proof of Proposition 2.2, with the only difference being the tempered likelihood. Specifically, by Bayes' theorem, the posterior distribution of the class probabilities for each observation satisfies

$$\begin{aligned}
\pi_{Y_i}^{\nu}(p_i) &\propto f_{p_{1:n}}(Y_{1:n})^{\nu} \pi(p_{1:n}) \\
&\propto f_{p_i}(Y_i)^{\nu} \pi(p_i) \\
&\propto \left(\prod_{k=1}^K p_i(k)^{\mathbb{I}(Y_i=k)} \right)^{\nu} \prod_{k=1}^K p_i(k)^{\alpha(k)-1}
\end{aligned}$$

$$= \prod_{k=1}^K p_i(k)^{\alpha(k) + \nu \mathbb{I}(Y_i=k) - 1}.$$

We recognize this as the kernel of a Dirichlet distribution with concentration parameters $\alpha + \nu e_{Y_i}$, which implies that

$$p_i \mid Y_{1:n} \sim \pi_{Y_i}^\nu = \text{Dir}(\alpha + \nu e_{Y_i}).$$

Furthermore, since the likelihood and prior factorize across observations, the joint posterior also factorizes:

$$\pi_{Y_{1:n}}^\nu(p_{1:n}) \propto f_{p_{1:n}}(Y_{1:n})^\nu \pi(p_{1:n}) \propto \prod_{i=1}^n f_{p_i}(Y_i)^\nu \pi(p_i) \propto \prod_{i=1}^n \pi_{Y_i}^\nu(p_i).$$

As a consequence, the posterior distribution of new class probabilities is equal to the prior:

$$\pi_{Y_{1:n}}^\nu(p_{n+1}) \propto \prod_{i=1}^n f_{p_i}(Y_i)^\nu \prod_{i=1}^{n+1} \pi(p_i) \propto \pi(p_{n+1}) = \text{Dir}(\alpha).$$

Finally, the posterior predictive distribution follows from Lemma B.1:

$$\begin{aligned} \mathbb{P}(Y_{n+1} = k \mid Y_{1:n}) &= \int \mathbb{P}(Y_{n+1} = k \mid p_{n+1}) \pi_{Y_{1:n}}^\nu(p_{n+1}) dp_{n+1} \\ &= \int p_{n+1}(k) \pi(p_{n+1}) dp_{n+1} \\ &= \mathbb{E}_\pi[p_{n+1}(k)] \\ &= \frac{\alpha(k)}{\alpha_0}. \end{aligned}$$

□

B.6 Proof of Theorem 2.10

Proof. Following the same steps as in the proof of Proposition 2.7, we can rewrite the variational objective as follows:

$$\begin{aligned} \text{KL}\left(q_{X_{1:n}}^\phi \parallel \pi_{Y_{1:n}}^\nu\right) &= \mathbb{E}_{q_{X_{1:n}}^\phi} \left[\log \frac{\prod_{i=1}^n q_{X_i}^\phi(p_i)}{\prod_{i=1}^n \pi_{Y_i}^\nu(p_i)} \right] \\ &= \sum_{i=1}^n \mathbb{E}_{q_{X_i}^\phi} \left[\log \frac{q_{X_i}^\phi(p_i)}{\pi_{Y_i}^\nu(p_i)} \right] \\ &\propto \sum_{i=1}^n \mathbb{E}_{q_{X_i}^\phi} \left[\log \frac{q_{X_i}^\phi(p_i)}{f_{p_i}(Y_i)^\nu \pi(p_i)} \right] \\ &= \sum_{i=1}^n -\nu \mathbb{E}_{q_{X_i}^\phi} [\log f_{p_i}(Y_i)] + \mathbb{E}_{q_{X_i}^\phi} \left[\log \frac{q_{X_i}^\phi(p_i)}{\pi(p_i)} \right] \end{aligned}$$

$$\begin{aligned}
&= \nu \sum_{i=1}^n -\mathbb{E}_{q_{X_i}^\phi} [\log f_{p_i}(Y_i)] + \frac{1}{\nu} \text{KL} \left(q_{X_i}^\phi \parallel \pi \right) \\
&= \nu \mathcal{L}^\nu(\phi; Y_{1:n}, X_{1:n}).
\end{aligned}$$

Therefore, since ν is a positive constant, we have that

$$\hat{\phi}_n = \arg \min_{\phi} \left\{ \text{KL} \left(q_{X_{1:n}}^\phi \parallel \pi_{Y_{1:n}}^\nu \right) \right\} = \arg \min_{\phi} \left\{ \mathcal{L}^\nu(\phi; Y_{1:n}, X_{1:n}) \right\}.$$

□

B.7 Proof of Proposition 2.11

Let us begin with the following lemma on the properties of the KL divergence, which is stated without proof, as it is a standard result.

Lemma B.2. *Properties of the Kullback-Leibler Divergence.* *Let f and g be two probability density functions defined on the same probability space. Then, the KL divergence from f to g is non-negative:*

$$\text{KL}(f \parallel g) \geq 0,$$

with equality if and only if f and g are equal almost surely.

Proof. By Theorem 2.10, we have that

$$\min_{\phi \in \Phi} \left\{ \mathcal{L}^\nu(\phi; Y_{1:n}, X_{1:n}) \right\} = \frac{1}{\nu} \min_{\phi \in \Phi} \left\{ \text{KL} \left(q_{X_{1:n}}^\phi \parallel \pi_{Y_{1:n}}^\nu \right) \right\}.$$

If the neural network class is sufficiently expressive to allow for the minimizer of the KL divergence and the optimization procedure actually achieves it, then by Lemma B.2, we have that

$$\text{KL} \left(q_{X_{1:n}}^{\hat{\phi}_n} \parallel \pi_{Y_{1:n}}^\nu \right) = 0,$$

which holds if and only if

$$q_{X_{1:n}}^{\hat{\phi}_n} = \pi_{Y_{1:n}}^\nu.$$

In turn, since both distributions factorize across observations, this is equivalent to requiring that

$$q_{X_i}^{\hat{\phi}_n} = \pi_{Y_i}^\nu, \quad \text{for } i = 1, \dots, n.$$

Finally, by the definitions of the variational distribution and the tempered posterior, this is equivalent to requiring that

$$\text{Dir}(\alpha + \text{NN}_{X_i}^{\hat{\phi}_n}) = \text{Dir}(\alpha + \nu e_{Y_i}), \quad \text{for } i = 1, \dots, n,$$

which holds if and only if

$$\text{NN}_{X_i}^{\hat{\phi}_n} = \nu e_{Y_i}, \quad \text{for } i = 1, \dots, n.$$

□

B.8 Proof of Proposition 2.13

By Definition 2.12, the vacuity of the approximate posterior predictive distribution is as follows:

$$\begin{aligned} u\left(\alpha + \text{NN}_{X_{n+1}}^{\hat{\phi}_n}\right) &= \frac{K}{\alpha_0 + \sum_{k=1}^K \text{NN}_{X_{n+1}}^{\hat{\phi}_n}(k)} \\ &= \frac{K}{\alpha_0 + \sum_{k=1}^K \nu e_{Y_{n+1}}(k)} \\ &= \frac{K}{\alpha_0 + \nu}, \end{aligned}$$

where we used the perfect interpolation condition from Proposition 2.11 in the second step.

B.9 Proof of Theorem 2.15

We can rewrite the empirical risk as follows:

$$\begin{aligned} \widehat{\mathcal{R}}_n^\nu(\phi) &= \frac{1}{n} \sum_{i=1}^n \text{KL}\left(q_{X_i}^\phi \parallel \pi_{Y_i}^\nu\right) \\ &= \frac{1}{n} \text{KL}\left(q_{X_{1:n}}^\phi \parallel \pi_{Y_{1:n}}^\nu\right) \\ &= \frac{\nu}{n} \mathcal{L}^{\frac{1}{\nu}}(\phi; Y_{1:n}, X_{1:n}), \end{aligned}$$

where in the last step we skipped the same steps as in the proof of Theorem 2.10.

B.10 Proof of Theorem 2.16

By the law of iterated expectations, we can rewrite the population risk as follows:

$$\begin{aligned} \mathcal{R}^\nu(\phi) &= \mathbb{E}_{P_X^*} \left[\mathbb{E}_{P_{Y|X}^*} \left[\text{KL}\left(q_X^\phi \parallel \pi_Y^\nu\right) \right] \right] \\ &= \mathbb{E}_{P_X^*} \left[\mathbb{E}_{P_{Y|X}^*} \left[\mathbb{E}_{q_X^\phi} \left[\log q_X^\phi(p) - \log \pi_Y^\nu(p) \right] \right] \right] \\ &= \mathbb{E}_{P_X^*} \left[\mathbb{E}_{q_X^\phi} \left[\log q_X^\phi(p) - \mathbb{E}_{P_{Y|X}^*} [\log \pi_Y^\nu(p)] \right] \right], \end{aligned}$$

where we interchanged the order of expectations in the last step, since the first term is independent of Y , and the second term involves an expectation over $P_{Y|X}^*$, which is a finite sum and can therefore be freely reordered with the expectation over the variational distribution.

Then, for each fixed X , by Gibb's variational principle, the population risk is minimized by choosing the parameter ϕ^* such that the variational distribution satisfies

$$q_X^{\phi^*} \propto \exp \left(\mathbb{E}_{P_{Y|X}^*} [\log \pi_Y^\nu(p)] \right)$$

$$\begin{aligned}
&= \exp \left(\mathbb{E}_{P_{Y|X}^*} [\log \text{Dir}(\alpha + \nu e_Y)] \right) \\
&= \exp \left(\mathbb{E}_{P_{Y|X}^*} \left[\sum_{k=1}^K (\alpha(k) + \nu e_Y(k) - 1) \log p(k) - \log B(\alpha + \nu e_Y) \right] \right) \\
&\propto \exp \left(\sum_{k=1}^K \left(\alpha(k) + \nu P_{Y|X}^*(k|X) - 1 \right) \log p(k) \right) \\
&= \prod_{k=1}^K p(k)^{\alpha(k) + \nu P_{Y|X}^*(k|X) - 1},
\end{aligned}$$

where B is the multivariate Beta function. We recognize this as the kernel of a Dirichlet distribution with concentration parameters $\alpha + \nu P_{Y|X}^*$. Therefore, we have that

$$q_X^{\phi^*} = \text{Dir} \left(\alpha + \nu P_{Y|X}^* \right).$$

B.11 Proof of Proposition 3.2

Under the variational approximation in Definition 3.1, the approximate posterior expectation of the class probabilities is

$$\begin{aligned}
\mathbb{E}[p_i | X_{1:n}, Y_{1:n}] &\approx \frac{\alpha + n \text{NF}_{X_i}^{\hat{\psi}_n} \text{NN}_{X_i}^{\hat{\psi}_n}}{\alpha_0 + n \text{NF}_{X_i}^{\hat{\psi}_n}} \\
&= \frac{\frac{\alpha}{n} + \text{NF}_{X_i}^{\hat{\psi}_n} \text{NN}_{X_i}^{\hat{\psi}_n}}{\frac{\alpha_0}{n} + \text{NF}_{X_i}^{\hat{\psi}_n}} \\
&\xrightarrow{p} \frac{P_X^*(X_i) P_{Y|X}^*(\cdot | X_i)}{P_X^*(X_i)} \\
&= P_{Y|X}^*(\cdot | X_i),
\end{aligned}$$

where the convergence in probability follows from the consistency of the two neural networks, as stated in Assumption 3.2 and the continuous mapping theorem. Similarly, the approximate posterior variance of the class probabilities is

$$\begin{aligned}
\text{Var}[p_i(k) | X_{1:n}, Y_{1:n}] &\approx \frac{\frac{\alpha + n \text{NF}_{X_i}^{\hat{\psi}_n} \text{NN}_{X_i}^{\hat{\psi}_n}(k)}{\alpha_0 + n \text{NF}_{X_i}^{\hat{\psi}_n}} \left(1 - \frac{\alpha + n \text{NF}_{X_i}^{\hat{\psi}_n} \text{NN}_{X_i}^{\hat{\psi}_n}(k)}{\alpha_0 + n \text{NF}_{X_i}^{\hat{\psi}_n}} \right)}{\alpha_0 + n \text{NF}_{X_i}^{\hat{\psi}_n} + 1} \\
&= \frac{\frac{\frac{\alpha}{n} + \text{NF}_{X_i}^{\hat{\psi}_n} \text{NN}_{X_i}^{\hat{\psi}_n}(k)}{\frac{\alpha_0}{n} + \text{NF}_{X_i}^{\hat{\psi}_n}} \left(1 - \frac{\frac{\alpha}{n} + \text{NF}_{X_i}^{\hat{\psi}_n} \text{NN}_{X_i}^{\hat{\psi}_n}(k)}{\frac{\alpha_0}{n} + \text{NF}_{X_i}^{\hat{\psi}_n}} \right)}{\alpha_0 + n \text{NF}_{X_i}^{\hat{\psi}_n} + 1} \\
&\xrightarrow{p} \frac{\frac{P_X^*(X_i) P_{Y|X}^*(k|X_i)}{P_X^*(X_i)} \left(1 - \frac{P_X^*(X_i) P_{Y|X}^*(k|X_i)}{P_X^*(X_i)} \right)}{\alpha_0 + n P_X^*(X_i) + 1}
\end{aligned}$$

$$\begin{aligned}
&= \frac{P_{Y|X}^*(k | X_i) \left(1 - P_{Y|X}^*(k | X_i)\right)}{\alpha_0 + n P_X^*(X_i) + 1} \\
&\rightarrow 0,
\end{aligned}$$

where the convergence in probability again follows from the consistency of the two neural networks and the continuous mapping theorem, while the final step follows from the fact that the denominator diverges to infinity as n goes to infinity.

Therefore, by Chebyshev's inequality, we have that

$$\mathbb{P}(|p_i(k) - \mathbb{E}[p_i(k) | X_{1:n}, Y_{1:n}]| > \varepsilon | X_{1:n}, Y_{1:n}) \leq \frac{\text{Var}[p_i(k) | X_{1:n}, Y_{1:n}]}{\varepsilon^2} \xrightarrow{n} 0.$$

Hence, we have that

$$\begin{aligned}
\mathbb{P}(\|p_i - \mathbb{E}[p_i | X_{1:n}, Y_{1:n}]\|_1 > \varepsilon | X_{1:n}, Y_{1:n}) &= \mathbb{P}\left(\sum_{k=1}^K |p_i(k) - \mathbb{E}[p_i(k) | X_{1:n}, Y_{1:n}]| > \varepsilon | X_{1:n}, Y_{1:n}\right) \\
&\leq \sum_{k=1}^K \mathbb{P}\left(|p_i(k) - \mathbb{E}[p_i(k) | X_{1:n}, Y_{1:n}]| > \frac{\varepsilon}{K} | X_{1:n}, Y_{1:n}\right) \\
&\xrightarrow{n} 0.
\end{aligned}$$

Finally, by the triangular inequality we have that

$$\begin{aligned}
\|p_i - P_{Y|X}^*(\cdot | X_i)\|_1 &\leq \|p_i - \mathbb{E}[p_i | X_{1:n}, Y_{1:n}]\|_1 + \|\mathbb{E}[p_i | X_{1:n}, Y_{1:n}] - P_{Y|X}^*(\cdot | X_i)\|_1 \\
&\xrightarrow{n} 0
\end{aligned}$$

Therefore, $p_i \xrightarrow{L_1} P_{Y|X}^*(\cdot | X_i) | X_{1:n}, Y_{1:n}$, which implies that $p_i \xrightarrow{p} P_{Y|X}^*(\cdot | X_i) | X_{1:n}, Y_{1:n}$.

Appendix C: Detailed Experimental Configuration

This appendix provides the precise model architectures, training hyperparameters, and data processing steps used in our experiments to ensure reproducibility. All experiments were conducted using the PyTorch framework [42] on a single NVIDIA GPU.

C.1 MNIST Configuration for DIP-EDL

For the MNIST dataset [13], we employ an architecture operating in pixel space. The density estimator is implemented using the `nflows` library [14].

Backbone Architecture (LeNet-5). We utilize a standard LeNet-style Convolutional Neural Network [32].

Density Estimator (MAF). We employ a Masked Autoregressive Flow (MAF) [41] to model the data density directly on flattened 28×28 pixel inputs. The flow consists

Table 4: LeNet-5 implementation details for MNIST.

Layer Type	Specifications
Conv2d	In: 1, Out: 20, Kernel: 5×5 , Stride: 1, Pad: 2, ReLU
MaxPool2d	Kernel: 2×2 , Stride: 2
Conv2d	In: 20, Out: 50, Kernel: 5×5 , Stride: 1, Pad: 0, ReLU
MaxPool2d	Kernel: 2×2 , Stride: 2
Flatten	Output Dimension: 1250 ($50 \times 5 \times 5$)
Linear	In: 1250, Out: 500, ReLU
Dropout	$p = 0.5$
Linear (Head)	In: 500, Out: 10 (No activation)

of 10 autoregressive layers, each containing 1024 hidden units. We utilize 20 blocks per layer and apply Batch Normalization between layers to improve convergence.

Data Augmentation & Preprocessing. For the density estimator, we adhere to the preprocessing protocol established in [41].

1. **Dequantization:** We add uniform noise $u \sim U(0, 1)$ to the discrete pixel values $x \in \{0, \dots, 255\}$ to convert them into continuous variables: $x' = (x + u)/256$.
2. **Logit Transformation:** To map the bounded data $x' \in [0, 1]$ to the unconstrained real space \mathbb{R} required by the flow, we apply a logit transformation:

$$z = \text{logit}(\lambda + (1 - 2\lambda)x')$$

where $\lambda = 10^{-6}$ is a regularization parameter to prevent numerical instability at the boundaries.

No standard mean/variance normalization or geometric augmentations (e.g., rotation) were applied to the MNIST data.

Training Hyperparameters.

Table 5: Training Hyperparameters for MNIST

Parameter	Backbone (EDL)	Density Estimator (MAF)
Optimizer	Adam	Adam
Batch Size	128	128
Epochs	50	50
Learning Rate	1×10^{-3}	1×10^{-4}
Weight Decay	5×10^{-3}	1×10^{-5}
Scheduler	None	StepLR (Step: 5, Gamma: 0.5)
Annealing Steps	10 Epochs	N/A

C.2 CIFAR-10 Configuration for DIP-EDL

For the more complex CIFAR-10 dataset [29], we utilize a ResNet-based backbone [23] and perform density estimation in the learned feature space.

Backbone Architecture (Modified ResNet-18). We adapt the ResNet-18 architecture to handle low-resolution 32×32 inputs. Specifically, the initial 7×7 convolution (stride 2) is replaced with a 3×3 convolution (stride 1), and the first max-pooling layer is removed to preserve spatial resolution. To enforce feature compactness, we apply Spectral Normalization (SN) to all convolutional layers in the backbone.

Density Estimator (GDA). We employ Gaussian Discriminant Analysis (GDA) on the 512-dimensional feature embeddings, adopting the official implementation from DAEDL [53]. We perform class-conditional multivariate Gaussian fitting ($C = 10$) in a post-hoc manner. After training the backbone, we freeze the weights and extract features for all ID training samples to compute the empirical mean and covariance matrix for each class. We utilize class-specific full covariance matrices (Quadratic Discriminant Analysis) to maximize density estimation precision.

Data Augmentation & Preprocessing. We apply standard data augmentations during training. These include random cropping to 32×32 with padding of 4, random horizontal flipping with a probability of 0.5, and random rotation of ± 15 degrees. All images are normalized using the standard CIFAR-10 mean and standard deviation ($\mu = (0.4914, 0.4822, 0.4465)$, $\sigma = (0.2023, 0.1994, 0.2010)$).

Training Hyperparameters (CIFAR-10).

Table 6: Training Hyperparameters for CIFAR-10

Parameter	Value
Optimizer	Adam
Batch Size	128
Epochs	100
Learning Rate	1×10^{-3}
Weight Decay	5×10^{-4}
Scheduler	Cosine Annealing ($T_{max} = 100$)
Annealing Steps (KL)	10 Epochs
Density Estimator	Fitted on frozen features (One-shot)

C.3 Addressing underflow in DIP-EDL due to log-likelihoods with large negative magnitudes.

To ensure numerical stability, we address the scale of the output log-likelihoods. Raw log-densities in high-dimensional pixel space can take on large negative magnitudes (e.g., < -1000), leading to numerical underflow when exponentiated and converted to evidence. We mitigate this by Z-score normalizing the log-likelihoods using the mean and standard deviation statistics calculated on the In-Distribution (ID) training set.

C.4 Baseline Implementation Details

To ensure a rigorous and fair comparison, we utilize the official open-source implementations provided by the authors for all competing methods. We align the backbone architectures (LeNet for MNIST, ResNet for CIFAR-10) where applicable to isolate the contribution of the uncertainty quantification mechanism. We compare against EDL [46], R-EDL [8], DAEDL [53], and PostNet [7]. The specific optimization hyperparameters for these baselines are detailed in Tables 7 and 8.

Table 7: Baseline Training Hyperparameters (MNIST)

Method	Epochs	Batch Size	LR	Optimizer	Specific Parameters
R-EDL	60	64	1×10^{-3}	Adam	$\lambda_1 = 1.0, \lambda_2 = 0.1$
DAEDL	50	64	1×10^{-3}	Adam	Reg=0.05, Dropout=0.5
PostNet	50	64	5×10^{-5}	Adam	Latent Dim=6, Radial Flow

Table 8: Baseline Training Hyperparameters (CIFAR-10)

Method	Epochs	Batch Size	LR	Optimizer	Specific Parameters
R-EDL	200	64	1×10^{-4}	Adam	$\lambda_1 = 1.0, \lambda_2 = 0.1$
DAEDL	100	64	1×10^{-3}	Adam	Reg=0.05, Dropout=0.5
PostNet	200	64	5×10^{-4}	Adam	Latent Dim=6, Radial Flow

Appendix D: Addressing why OOD Brier Score is larger than expected on CIFAR-10 experiments for DIP-EDL. And why this is not the case for MNIST experiments.

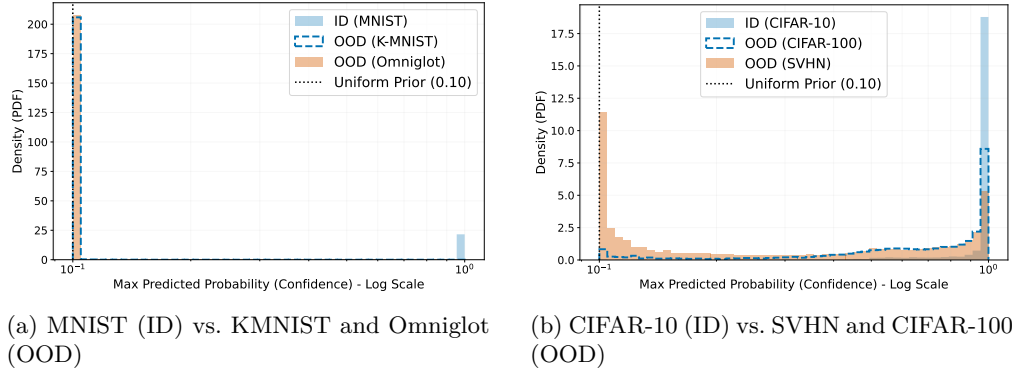


Figure 1: **Confidence Distributions for DIP-EDL.** *Left:* DIP-EDL demonstrates a near-perfect performance on MNIST where OOD samples collapse to the uniform prior (0.1). *Right:* On CIFAR-10, DIP-EDL shows a high-confidence tail for OOD samples, while remaining confident on ID data. This demonstrates the density estimator’s ability to differentiate between the two but struggle to capture all the details of complex, high-dimensional datasets, and explains the higher Brier Score despite good AUROC results.

Appendix E: Ablation study - full results

Table 9: Full results of the ablation study of DIP-EDL.

(a) MNIST (ID) vs. K-MNIST and Omniglot (OOD)

Components	ID Performance		OOD Performance Metrics								
	n	DE $_{X_i}^{\psi}$	NN $_{X_i}^{\phi}$	AUROC (↑)		AUPR (↑)		OOD BS (↓)			
				Acc. (↑)	BS (↓)	K-MNIST	Omniglot	K-MNIST	Omniglot		
✓	✓	✗		0.0980	0.9000	0.9998	0.9998	0.9996	0.9997	0.0000	0.0000
✓	✗	✓		0.9958	0.0069	0.5138	0.5299	0.5742	0.6408	0.6826	0.7124
✗	✓	✓		0.9952	0.7202	0.9996	0.9996	0.9992	0.9994	0.0000	0.0000
✓	✓	✓		0.9955	0.0079	0.9998	0.9998	0.9995	0.9997	0.0014	0.0000
✓	✗	✗		0.0980	0.9000	0.5000	0.5000	0.5000	0.5686	0.0000	0.0000
✗	✓	✗		0.0980	0.9000	0.9997	0.9997	0.9993	0.9995	0.0000	0.0000
✗	✗	✓		0.9958	0.7446	0.5076	0.5174	0.5386	0.6021	0.0056	0.0059

(b) CIFAR-10 (ID) vs. CIFAR-100 and SVHN (OOD)

Components	ID Performance		OOD Performance Metrics								
	n	DE $_{X_i}^{\psi}$	NN $_{X_i}^{\phi}$	AUROC (↑)		AUPR (↑)		OOD BS (↓)			
				Acc. (↑)	BS (↓)	CIFAR-100	SVHN	CIFAR-100	SVHN		
✓	✓	✗		0.1000	0.9000	0.8127	0.9143	0.7937	0.9577	0.0000	0.0000
✓	✗	✓		0.9179	0.1337	0.4742	0.4835	0.4888	0.7165	0.6910	0.7018
✗	✓	✓		0.9179	0.8259	0.8127	0.9143	0.7937	0.9577	0.0003	0.0001
✓	✓	✓		0.9179	0.1330	0.8127	0.9143	0.7937	0.9577	0.6324	0.5395
✓	✗	✗		0.1000	0.9000	0.5000	0.5000	0.5000	0.7225	0.0000	0.0000
✗	✓	✗		0.1000	0.9000	0.8127	0.9143	0.7937	0.9577	0.0000	0.0000
✗	✗	✓		0.9179	0.7596	0.5039	0.4981	0.5122	0.7225	0.0057	0.0058